Lyman line ratios in charge-exchange collisions of C^{6+} and O^{8+} ions with hydrogen and krypton atoms

Anthony C. K. Leung* and Tom Kirchner†
Department of Physics and Astronomy, York University, Toronto, Ontario M3J 1P3, Canada

(Received 15 May 2018; published 22 June 2018)

Charge-exchange collisions of C^{6+} and O^{8+} ions with hydrogen and krypton atoms followed by radiative emissions are examined using the two-center basis generator method in the low- and intermediate-energy regimes. Capture cross sections are obtained within the independent-electron model and are used in a radiative cascade model to yield Lyman line-emission counts. The main focus of this analysis is on single-electron capture with the inclusion of autoionizing double capture in krypton collisions. Because hydrogen and krypton have the same first ionization potential, it is expected from the classical overbarrier model that the capture selectivity of these two atoms is the same, making krypton a good surrogate for hydrogen to study collision-induced radiative emissions in the laboratory. However, the present analysis shows that the subshell distributions with respect to the impact energy in krypton collisions can differ from hydrogen collisions and, hence, from predictions of the classical overbarrier model. Based on the comparison of present results with previous measurements, this difference in capture behavior of the two target atoms does not appear problematic for the Lyman line-emission results for C^{6+} collisions, but does appear to affect these results for O^{8+} collisions.

DOI: 10.1103/PhysRevA.97.062705

I. INTRODUCTION

Collision-induced radiative emissions have been studied by many groups since the discovery of strong x-ray production from cometary gases [1]. Although it has been established that charge exchange between highly charged solar-wind ions and neutrals is the primary mechanism for the observed emissions [2,3], much work is needed to understand the details as there is useful astrophysical information that can be extracted, such as plasma composition abundances [4], density and composition of neutral gases [5], and general properties of ions, atoms, and molecules [6]. Being able to accurately quantify such a process can also help remove x rays in satellite observations as an undesired background [5].

Several groups have studied these charge-exchange collisions in the laboratory where capture cross sections and the corresponding radiative emissions were measured [7–16]. Recently, measurements of Lyman line emissions from C^{6+}-Kr collisions by Andrianarijaona *et al.* [17] and O^{8+}-Kr collisions by Seely *et al.* [18] in the low and intermediate impact-energy regimes were reported. The main focus of these studies is single-electron capture (SEC). Because of the absence of theoretical data at the time when these measurements were reported, comparisons of these measurements were made with those corresponding to cross sections of H collisions from previous calculations [19,20].

The comparison of the line emissions between H and Kr collisions is justified because the first ionization potential of the H atom (13.6 eV) is very similar to that of the Kr atom (14.0 eV). The classical overbarrier model (OBM) [21] suggests that they have the same n-state capture selectivity, which makes Kr a good surrogate for H atoms to study in the laboratory [17]. However, the actual comparisons [17,18] showed that the agreement is not always consistent, which likely indicates different l selectivity of the two targets. Moreover, the accuracy of previously calculated cross sections of H collisions [19,20] may also be questionable given the practical limitations (e.g., small basis-set sizes). To provide better insights into these measurements, it would be ideal to compare with results from direct calculations of Kr collisions and new calculations of H collisions.

In this article, we present results of a theoretical analysis[1] of C^{6+} and O^{8+} collisions with Kr and H atoms. It is based on the nonperturbative, coupled-channel two-center basis generator method (TC-BGM) [23] performed within the independent-electron model (IEM). Previously, we investigated other collision-induced radiative emissions [24–27] and found that the TC-BGM is applicable to these problems. However, collisions involving an atom as heavy as Kr has yet to be reported using this approach. Therefore, the recent Lyman line measurements of Kr collisions [17,18] serve as excellent benchmarks for the present study. We first discuss the IEM approach of the TC-BGM in Sec. II. In Sec. III, results of capture cross sections and Lyman line-emission ratios are presented and discussed. Finally, we present our concluding remarks in Sec. IV. Atomic units ($\hbar = e = m_e = 4\pi\epsilon_0 = 1$) are used throughout the article unless stated otherwise.

*leungant@yorku.ca
†tomk@yorku.ca

[1]Originally used as materials in the dissertation by A.C.K.L. [22].

II. THEORETICAL METHOD

A. Collision description

Theoretical calculations on all collision systems in this study are performed within the semiclassical approach where the projectile travels in a straight-line path at constant speed v_P described by $\mathbf{R}(t) = (b,0,v_P t)$, where b is the impact parameter. In the framework of the IEM, the time-dependent Schrödinger equation (TDSE) separates into a set of single-particle equations,

$$i\,\partial_t \psi_i(\mathbf{r},t) = \hat{h}(t)\psi_i(\mathbf{r},t),\ \ i = 1,\ldots,N, \tag{1}$$

with the single-particle Hamiltonian

$$\hat{h}(t) = -\frac{1}{2}\nabla^2 + V_P(|\mathbf{r}_P|) + V_T(|\mathbf{r}|,t), \tag{2}$$

where V_P and V_T are the interaction potentials of a single electron with the projectile and target, respectively. The position vector of the electron with respect to the projectile $\mathbf{r}_P$ is related to that with respect to the target by $\mathbf{r}_P(t) = \mathbf{r} - \mathbf{R}(t)$.

More precisely, V_P is the Coulomb potential with nucleus charge number $Z = 6$ and $Z = 8$ for C^{6+} and O^{8+}, respectively. As for V_T corresponding to the H atom, it is given by a Coulomb potential with $Z = 1$. For Kr, an effective ground-state potential was obtained from the optimized potential method (OPM) of Talman and co-workers [28,29]. The effective potential obtained from the OPM includes the electron-nucleus Coulomb interaction, screening, and exchange terms. As a consequence, it exhibits the correct asymptotic behavior (i.e., $-1/r$). The total target potential of Kr is summarized as

$$V_{Kr}(|\mathbf{r}|,t) = -\frac{36}{r} + v_{ee}(r,t), \tag{3}$$

where

$$v_{ee}(r,t) = v^0_{ee}(r) + \delta v_{ee}(r,t) \tag{4}$$

is an effective mean-field potential that models the electron-electron interaction on the exchange-only level. Two variants of this mean-field potential are considered: (i) the *no-response* approximation, where the ground-state potential remains frozen during the course of the collision (i.e., $\delta v_{ee} = 0$), and (ii) a *target-response* model [30], which takes into account a time-dependent screening potential due to electron removal during the collision. This screening model assumes the form

$$\delta v_{ee}(r,t) = -\frac{Q_s(t)}{N-1} v^0_{ee}(r), \tag{5}$$

where Q_s is a time-dependent screening function that depends on electron loss [30]. The inclusion of this screening model has been shown to be important in the low- and intermediate-energy regimes in producing more reliable total cross sections [26,31,32] than the no-response approximation.

The set of single-particle TDSEs (1) is solved by projecting them onto a finite set of basis states and propagating them using the TC-BGM. In this study, the TC-BGM basis sets $\{\chi^\mu_\nu\}$ include nlm hydrogenlike states from $n = 1$ to $n = 7$ of the projectiles, all states in the $KLMN$ shells of the H atom, and all states in the MNO shells of Kr. For Kr, test calculations showed that electron capture from the M shell is negligible, and thus all states in the K and L shells can be safely neglected in the present study. Moreover, a set of BGM pseudostates was also included to account for quasimolecular couplings and transitions to the continuum. These states are generated from the target atomic orbitals $\{\phi^0_\nu\}$ by repeated application of a regularized projectile potential [33],

$$W_P(t) = \frac{1 - \exp[-|\mathbf{r}_P(t)|]}{|\mathbf{r}_P(t)|}, \tag{6}$$

such that the BGM pseudostates

$$\chi^\mu_\nu(\mathbf{r},t) = [W_P(t)]^\mu \phi^0_\nu(\mathbf{r},t),\ \ \mu = 1,\ldots,M_\nu, \tag{7}$$

are dynamically adapted to the problem at hand. For two-center collision calculations, all basis states are endowed with electron translation factors to ensure Galilean invariance [23].

The single-particle equations are solved to yield the single-particle probabilities for capture p^{cap} and ionization p^{ion}. For the many-electron ion-Kr systems, single-particle probabilities are combined statistically in order to obtain a proper representation of the experimental observable. Within the IEM, one can utilize the shell-specific multinomial analysis to obtain q-fold capture with simultaneous k-fold ionization [34,35]. The main focus here is on capture with no ionization (i.e., $k = 0$). The corresponding multinomial analysis for this observable is then

$$P^{q0} = \sum_{q_1,\ldots,q_m}^{N_1,\ldots,N_m} \prod_{i=1}^{m} \binom{N_i}{q_i} \left(p_i^{cap}\right)^{q_i} \times \left(1 - p_i^{cap} - p_i^{ion}\right)^{N_i - q_i} \delta_{q,\sum_i q_i}, \tag{8}$$

where m is the number of electron shells and N_i is the number of electrons in the ith shell. The Kronecker δ ensures that only q-fold capture events are summed up. Furthermore, we considered $q = 1$ which we refer to as *pure* SEC. The case of $q = 2$ was also considered to account for autoionizing double capture (ADC) to the overall single-capture events. It was found from the present IEM analysis that contributions from autoionizing triple capture to the overall SEC events are not important for the postcollision analysis (specifically, total cross sections of $<15\%$ with respect to pure SEC), and so capture events of $q \geqslant 3$ were not considered. This is consistent with the observations of a coincidence experiment of triple-electron capture for krypton collisions by Martin *et al.* [36].

Once the multinomial calculation has been carried out, the capture cross section is obtained by

$$\sigma_{cap} = 2\pi \int_0^\infty b\,P^{q0}(b)db. \tag{9}$$

The capture cross sections serve as initial conditions for the postcollision analysis.

B. Lyman line emissions

Once electrons from the target are captured into excited states of the projectile, they may subsequently transit to the lowest unoccupied bound state. Here we consider radiative decay from pure SEC and those including ADC. In a first-principles approach, the population N of some level p is

governed by [37,38]

$$\frac{dN_p(t)}{dt} = \sum_{i=p+1}^{m} N_i(t)A_{i\to p} - N_p(t)\sum_{f=i}^{p-1} A_{p\to f}, \qquad (10)$$

where A is a transition probability per unit time. The first summation on the right-hand side of Eq. (10) is the rate of repopulation of level p from a cascade in higher levels i and the second sum is the rate of depopulation into lower levels f. The population level index is a multi-index in practice and transitions can occur through intermediate states dictated by selection rules (e.g., $|l - l'| = 1$ for radiative dipole decay).

Radiative transition rates can be calculated analytically for the hydrogenlike C^{5+} and O^{7+} ions. The present analysis only considers radiative transitions according to the electric-dipole selection rule. Starting from Fermi's golden rule in the electric-dipole approximation, one obtains [25]

$$A^{\rm rad}_{nl\to n'l'} = \frac{4}{3}\left(\frac{\omega_{nn'}}{c}\right)^3 (2l'+1)\begin{pmatrix} l' & 1 & l \\ 0 & 0 & 0\end{pmatrix}^2 \times\left(\int_0^\infty R_{nl}R_{n'l'}r^3 dr\right)^2, \qquad (11)$$

where $\omega_{nn'}$ is the transition frequency and R_{nl} is the radial wave function for the hydrogenlike ions. As for accurate calculations of Auger decay rates, we used the AUGER component of the RATIP program [39] to perform such calculations numerically since seeking for analytic forms of doubly excited states is not viable. The RATIP program provides *ab initio* calculations of the electronic structure and properties of atom and ions. Although RATIP utilizes the multiconfiguration Dirac-Fock method, the present analysis is restricted to single configurations to be consistent with the IEM framework. The interaction among the electrons in the transition amplitude calculation performed in AUGER is restricted to the instantaneous Coulomb repulsion.

Once the populations are solved, we obtain the total photon counts by integrating the intensity expression [38]

$$(\text{counts})_{nl\to n'l'} = A^{\rm rad}_{nl\to n'l'}\int_0^\infty N_{nl}(t)dt. \qquad (12)$$

The present focus is on photon counts that correspond to the Lyman series (i.e., $n \geqslant 2 \to n = 1$ transitions) from Ly-α to Ly-ϵ.

III. RESULTS AND DISCUSSION

A. C^{6+} collisions with H and Kr

The results of SEC cross sections from C^{6+} collisions are shown in Fig. 1. Specifically, cross sections of C^{6+}-H collisions are shown in Fig. 1(a), where the present TC-BGM results are compared with recommended values [40]. In Fig. 1(b), we show cross sections of C^{6+}-Kr collisions from various present IEM calculations for pure SEC and total SEC (i.e., pure SEC + ADC). Using the multinomial analysis, cross sections from the no-response approximation and using the response model are shown.

Beginning the discussion with H collisions [Fig. 1(a)], the present cross sections are consistent with the recommended values. The cross sections do not vary significantly between 0.5 and 20 keV/amu, but decrease for $E_{\rm P} > 20$ keV/amu since other electronic processes such as ionization are important at higher energies. This is a general behavior seen in collision systems in the same energy range [41]. In close examination, the present cross sections mostly lie within the uncertainties of the recommended values except at 0.5 keV/amu. This is a likely indication that the straight-line assumption may not be sufficient since deflection due to internuclear repulsion is not negligible at such low energies. Overall, the present cross sections for this collision system are deemed satisfactory.

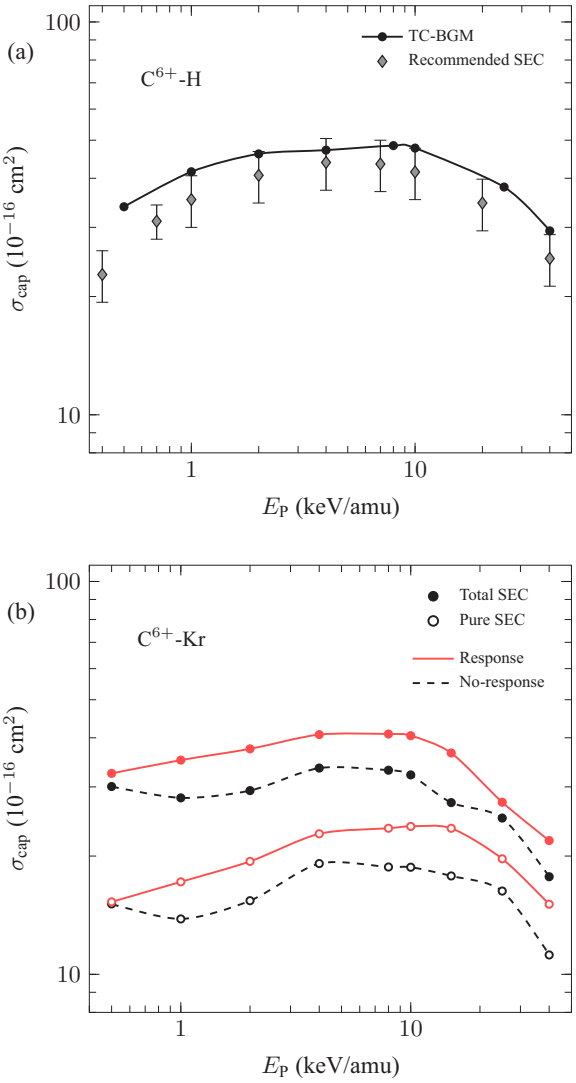

FIG. 1. Capture cross sections plotted with respect to impact energy: (a) C^{6+}-H collisions from present calculations and recommended SEC from Janev *et al.* [40], and (b) C^{6+}-Kr collisions from present TC-BGM calculations.

Next, with Kr collisions [Fig. 1(b)], the present cross sections also show a similar behavior with respect to the impact energy and do not vary significantly from 0.5 to 15 keV/amu, but do decrease for $E_{\rm P} > 15$ keV/amu. Comparisons reveal some differences between results using the no-response approximation and those using the target-response model, similar to what was observed in previous TC-BGM analyses on slow collisions [26,31,32]. If one were to compare these cross sections with those of H collisions [Fig. 1(a)], results from

calculations using the response model which include ADC are most similar. The present results also show a considerable contribution of ADC towards the overall SEC events.

In a more detailed examination of the present IEM results, we have found that ADC mainly contributes to the capture population of the $n = 2$ and $n = 3$ states of the projectile. It was determined, from calculations that use the response model, that the cross-section ratios of ADC to pure SEC are, for example, 0.94, 0.69, and 0.49 at 1, 4, and 10 keV/amu, respectively. The corresponding ratios in the no-response approximation are 0.84, 0.55, and 0.46. According to the coincidence collision experiment on two-electron capture by Chen *et al.* [42], these ratios for C^{6+}-Kr collisions are deduced to be 0.53, 0.26, and 0.24 at 1, 5, and 9.5 keV/amu, respectively, i.e., the proportions of ADC produced in the present IEM analysis appear overestimated.

In Fig. 2, the n-state relative cross-section $\sigma_n^{\rm rel} = \sigma_n/\sigma_{\rm total}$ distributions corresponding to impact energies of 1, 8, and 25 keV/amu are shown. For this discussion, only cross sections of pure SEC are presented. Starting with H collisions [Fig. 2(a)], the distribution at 1 keV/amu shows a very selective profile where capture primarily occurs into the $n = 4$ state of the projectile. This primary capture state can be verified using the OBM. At higher impact energies, one can see that the n distribution broadens, a general behavior of capture when transitioning from the low- to intermediate-energy regimes [41].

Similar n selectivity of capture is also shown for Kr collisions [Fig. 2(b)]. Specifically, at 1 keV/amu, the distribution shows that the main capture channel is $n = 4$. However, at 8 keV/amu, the present calculations reveal a degeneratelike n distribution, showing a fairly even population in the $n = 4$ and $n = 5$ capture channels while the populations of all other states are negligible. At an even higher energy of 25 keV/amu, the expected broadened profile is obtained with the population being peaked at $n = 5$. This change in the primary capture channel in H vs Kr collisions could be explained using energy-correlation diagrams where one might expect to see different avoided crossings from the two targets since capture from the H atom occurs from the $1s$ shell, while capture from Kr mainly occurs from the $4p$ shell. On the other hand, energy-correlation diagrams may not fully explain this capture behavior as it appears to be dependent on the impact energy, which is beyond this type of analysis.

Moving on to the radiative emission results, Fig. 3 shows the Lyman line-emission ratios from C^{6+}-H and -Kr collisions. All calculated ratios in the figure are from the present TC-BGM calculations. For Kr collisions, we show results from different IEM calculations. Specifically, not only are they separated between using the no-response approximation and the response model, but they are also separated by pure SEC and total SEC events. All calculated ratios are compared with the experimental results for C^{6+}-Kr collisions by Andrianarijaona *et al.* [17].

Examining first the two dominant ratios of Ly-β/Ly-α and Ly-γ/Ly-α, the profiles of these obtained ratios are very similar to the experimental ratios for both Kr and H collisions. Specifically, the ratios appear fairly constant from 0.5 to 4 keV/amu and decrease toward higher energies. The decreasing behavior of the ratios can be understood from the increasing

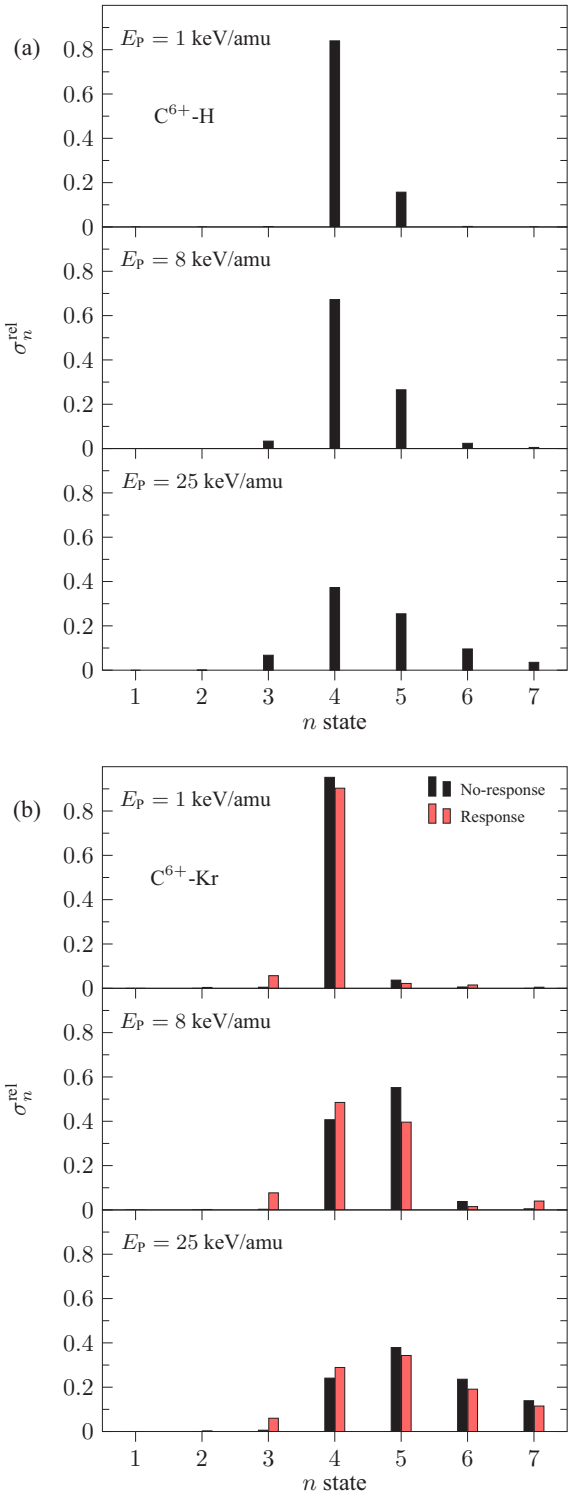

FIG. 2. n-state selective relative capture cross-section distributions at $E_P = 1$, 8, and 25 keV/amu for (a) C^{6+}-H collisions and (b) C^{6+}-Kr collisions.

capture population of the maximum l subshell as collision energy increases [41], thereby increasing the Ly-α counts by the yrast cascade [38]. This behavior of line-emission ratios was also seen in other collision systems in previous studies [15,26]. Furthermore, one can see the range of results that can

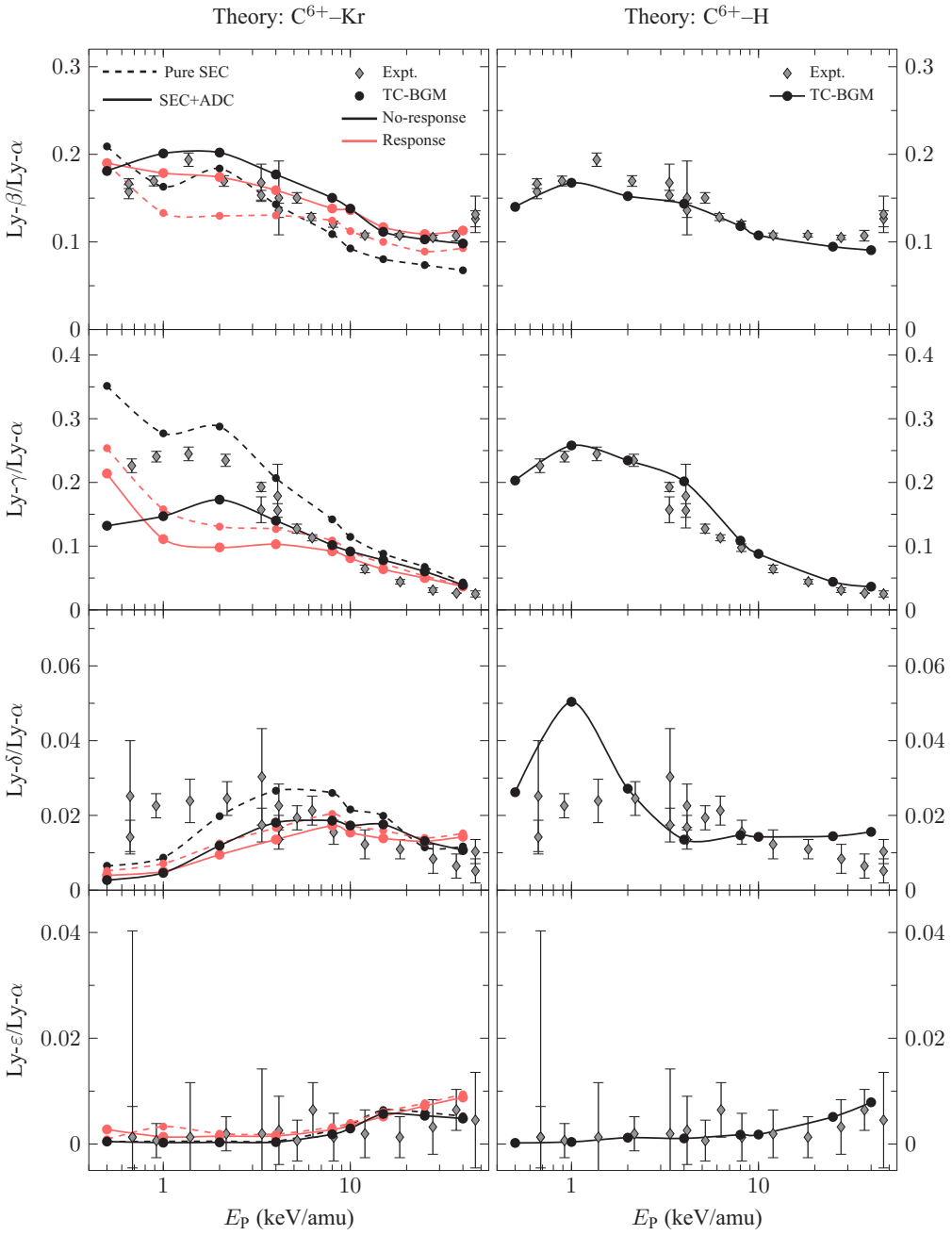

FIG. 3. Lyman line-emission ratios of Ly-β/Ly-α, Ly-γ/Ly-α, Ly-δ/Ly-α, and Ly-ϵ/Ly-α. Calculated TC-BGM ratios from C^{6+}-Kr (left column) and C^{6+}-H (right column) collisions. Experimental ratios [17] in both columns correspond to C^{6+}-Kr collisions only.

be obtained through different variants of IEM calculations for Kr collisions. In particular, calculated line-emission profiles of Kr collisions which include ADC events are qualitatively most similar to the experimental results, demonstrating the importance of these capture events for radiative emissions. The remaining quantitative differences are attributed to the overestimation of the ADC cross sections, as discussed above.

For the subdominant ratios of Ly-δ/Ly-α and Ly-ϵ/Ly-α, the present results of Kr collisions also show good agreement with the experimental values. The small magnitude of all these ratios is simply due to small capture populations of np states for $n \geqslant 5$ at these energies. Similar agreement is also shown for the present calculations of H collisions but with a few exceptions in the Ly-δ/Ly-α ratios, for example, at 1 keV/amu. We also note that these ratios produced from the present cross sections of hydrogen collisions are closer to the experimental ratios for Kr than those based on the recommended partial cross sections of Ref. [20], which Andrianarijaona *et al.* [17] had presumably used in their radiative cascade calculations to compare with the experimental ratios (which are not shown here).

B. O^{8+} collisions with H and Kr

To assess the present results for O^{8+} collisions, Fig. 4 shows the SEC cross sections plotted with respect to the impact energy. The focus here is on impact energies between 0.5 and

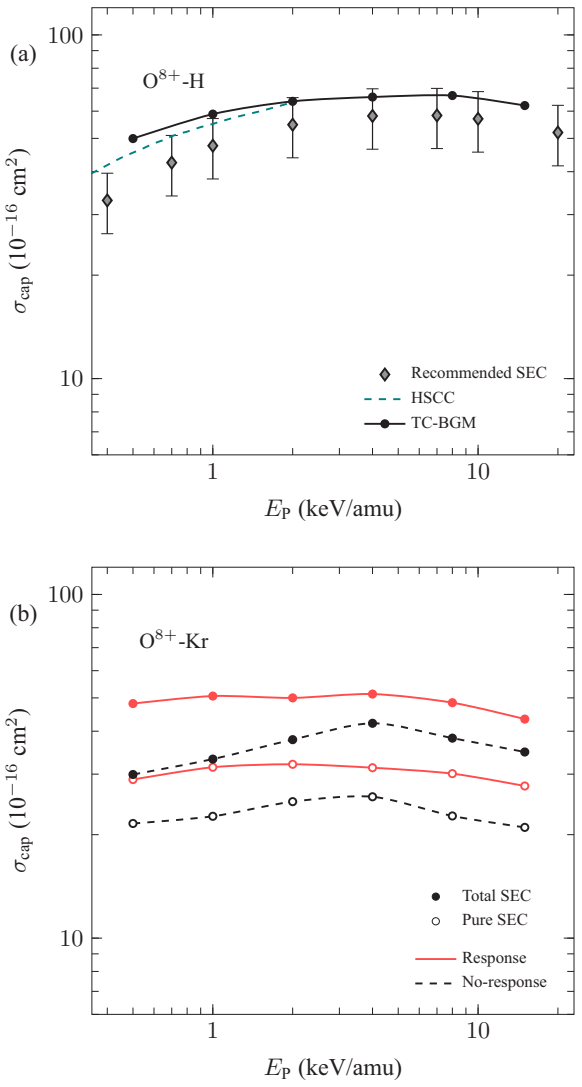

FIG. 4. Capture cross sections with respect to impact energy: (a) O^{8+}-H collisions from present calculations, HSCC results [43], and recommended SEC [40]; (b) O^{8+}-Kr collisions from present TC-BGM calculations.

15 keV/amu. Results of O^{8+}-H collisions are shown in Fig. 4(a), while results of O^{8+}-Kr collisions are shown in Fig. 4(b).

The present cross sections for O^{8+}-H collisions are compared with the recommended values [40] and results from a hyperspherical close-coupling (HSCC) calculation by Lee *et al.* [43], showing overall consistency. The slight quantitative discrepancy of the cross-section profiles between the present calculations and those from the HSCC calculations is most likely due to the straight-line approximation that was employed in the present calculations. Considering that this discrepancy is less than 10% at the lowest impact energy of 0.5 keV/amu, the straight-line approximation used in the TC-BGM calculations is not viewed as problematic for the radiative analysis.

For O^{8+}-Kr collisions, the total cross sections shown in Fig. 4(b) are separated by the different IEM calculations. All of these cross sections show little variation with respect to impact energy. When these results are compared with those of

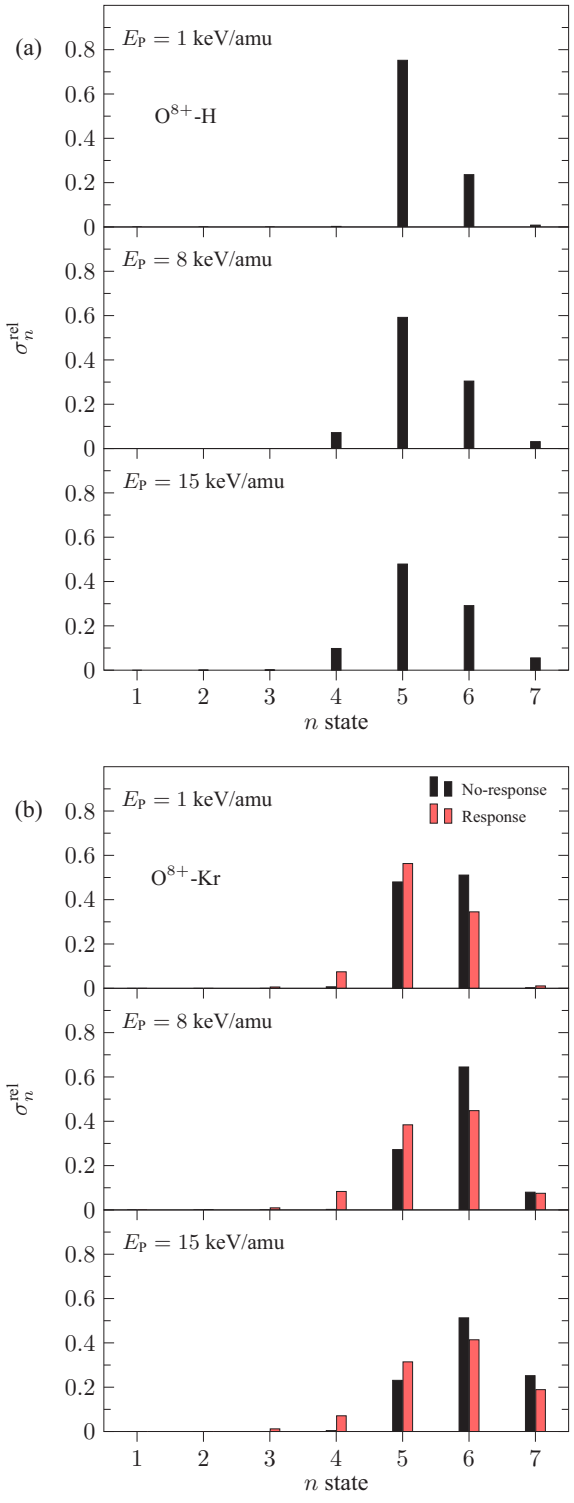

FIG. 5. n-state selective relative capture cross-section distributions at E_P = 1, 8, and 25 keV/amu for (a) O^{8+}-H collisions and (b) O^{8+}-Kr collisions.

the H collisions of Fig. 4(a), one can see that the calculations of Kr collisions that correspond to the target-response model and include ADC are most similar to the former.

Similar to the C^{6+} collision analysis in Sec. III A, one can use the coincident experiment analysis by Martin *et al.* [44] to help assess the ADC proportion produced from the

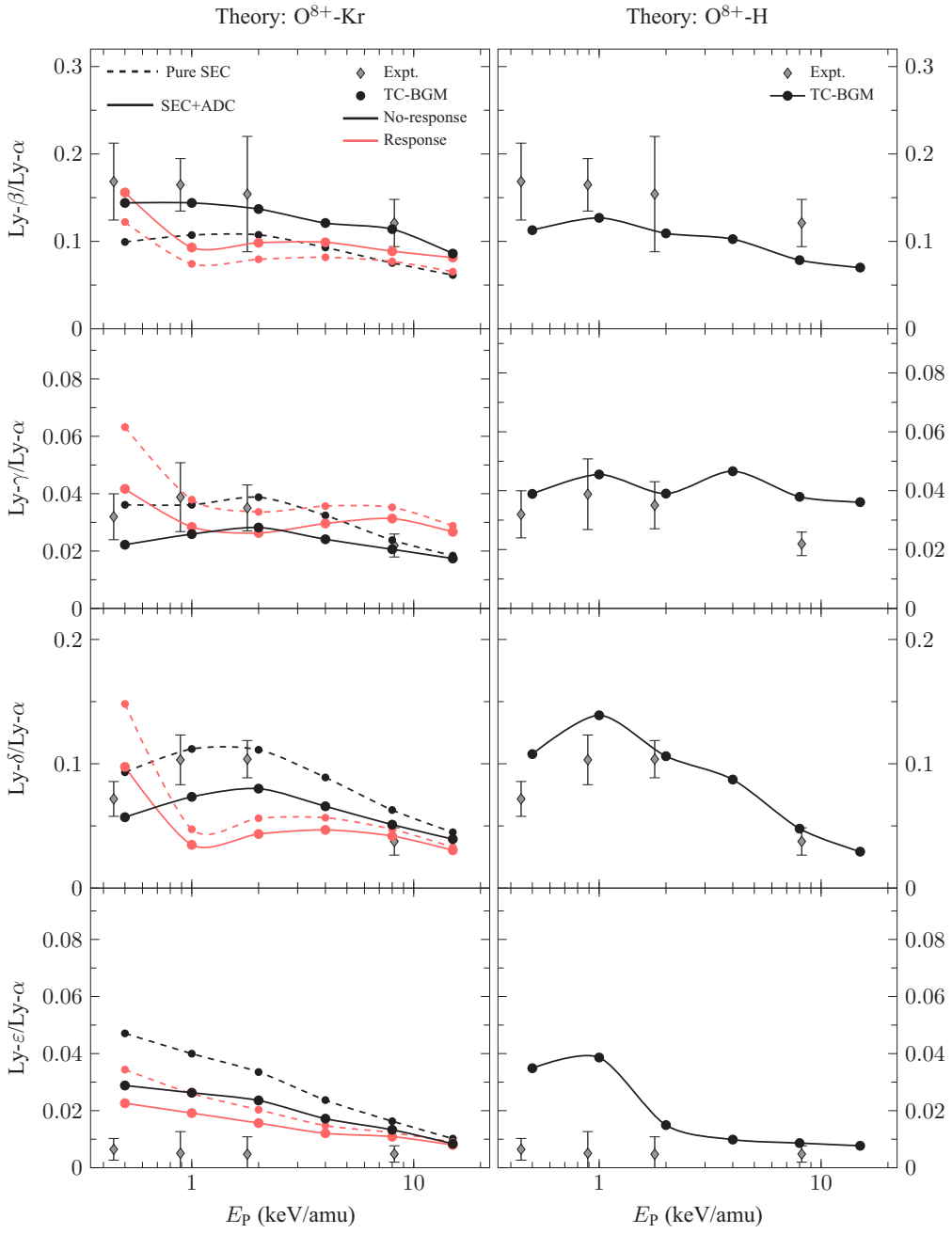

FIG. 6. Lyman line-emission ratios of Ly-β/Ly-α, Ly-γ/Ly-α, Ly-δ/Ly-α, and Ly-ϵ/Ly-α. Calculated TC-BGM ratios from O^{8+}-Kr (left column) and O^{8+}-H (right column) collisions. Experimental ratios [18] in both columns correspond to O^{8+}-Kr collisions only.

present calculations for O^{8+}-Kr collisions. First, we note that the present Auger analysis showed contributions to the single-capture population of the $n = 3$ and $n = 4$ states of the projectile, but mostly of the former. At 1 keV/amu, the ratio of ADC to pure SEC from the present calculations is 0.61 and 0.46 using the response model and the no-response approximation, respectively. From the coincidence experiment by Martin *et al.* [44], the corresponding ratio was deduced to be 0.44. This is an indication that the ADC proportion from calculations using the response model is too large.

Figure 5 shows the n-state relative cross-section distributions of pure SEC corresponding to impact energies of 1, 8, and 15 keV/amu. Figure 5(a) corresponds to collisions with H atoms and Fig. 5(b) corresponds to Kr collisions.

Starting with the n distribution from H collisions [Fig. 5(a)] at 1 keV/amu, one can see that the primary capture channel is $n = 5$, which is consistent with the OBM. At higher impact energies, one can see the broadening behavior of the n distribution [41].

For the n distribution from Kr collisions [Fig. 5(b)], one sees a degeneratelike profile starting at 1 keV/amu, which is unexpected based on the OBM. At higher energies, one sees the usual broad n distribution, but the peak resolves at $n = 6$, which is clearly different from H collisions [cf. Fig. 5(a)]. This

is the same behavior that was shown in C^{6+}-Kr collisions (cf. Sec. III A) but at somewhat different impact energies. This suggests that the projectile ion charge has an influence on this capture behavior. Moreover, this behavior is not exclusive to Kr collisions as it was also observed experimentally in Ar^{8+}-H collisions at about 2 keV/amu by Edgu-Fry *et al.* [45] and in the HSCC calculation by Lee *et al.* [43] for O^{8+}-H collisions but at a much lower impact energy of about 100 eV/amu.

Results of the Lyman line-emission ratios from O^{8+}-H and -Kr collisions are shown in Fig. 6. All calculated ratios in the figure are from the present TC-BGM calculations. To see the range of results, ratios from Kr collision calculations using different variants of the IEM are presented. All calculated ratios are compared with the experimental ratios of O^{8+}-Kr measurements by Seely *et al.* [18].

Examining the calculated line-emission ratios from Kr collisions, results based on the no-response approximation show the most consistent behavior with the experimental ratios. Specifically, the ratios tend to decrease with impact energy. Similar to the ratios from C^{6+} collisions (cf. Sec. III A), the decreasing profile is due to an increase in relative population in the maximum l subshell which increases the Ly-α count by the yrast cascade. Although produced ratios that include ADC would be consistent with the experiment [18], ratios from pure SEC also show good agreement with the measurements, with the exception of Ly-ϵ/Ly-α. Moreover, one can see that the ratios produced from calculations (e.g., Ly-γ/Ly-α) using the response model are comparable in magnitude with the experimental ratios, but show a different impact-energy profile.

The calculated line-emission ratios of H collisions are in overall mixed agreement with the experimental ratios of Kr collisions, which is a different observation compared to C^{6+} collisions. Specifically, the only ratio that is comparable with the Kr case is Lyβ/Ly-α. This was also demonstrated by Seely *et al.* [18] using the recommended cross sections for H collisions [20]. On the other hand, one should not be surprised by this observation given the different capture distributions that were obtained in these two different systems, as seen in Fig. 5. From all these comparisons, together with the results for C^{6+} collisions, one should not expect capture from the Kr atom to be identical to that from the H atom despite the expectations of the OBM.

IV. CONCLUSIONS

In this study, Lyman line-emission ratios from charge-exchange collisions of C^{6+} and O^{8+} ions with H and Kr were obtained using the TC-BGM performed within the IEM. Specifically, different sets of single-capture cross sections were obtained using this approach. In addition, comparisons of cross sections and n distributions were made between collisions with the two target atoms using the same projectile ion. The experimental ratios of Andrianarijaona *et al.* [17] and Seely *et al.* [18] served as a testbed for the present analysis.

For C^{6+} collisions with H and Kr, the present results showed different behaviors in the n distribution of the two targets with respect to the impact energy. Despite this difference, similar line-emission ratios from 0.5 to 40 keV/amu, particularly for Ly-β/Ly-α, Ly-γ/Ly-α, and Ly-ϵ/Ly-α, were obtained for collisions with these two target atoms. The present results also showed the importance of ADC towards the overall line-emission counts for the Kr atom, as is also the case for other charge-exchange collisions involving a many-electron target [9,13,15].

Similar observations from the comparison of the n distributions were also made for O^{8+} collisions with H and Kr from 0.5 to 15 keV/amu. In this case, however, the line-emission ratios corresponding to H collisions are somewhat different from Kr collisions, with the exception of Ly-β/Ly-α. All these findings suggest that using Kr as a surrogate for H atoms in slow, highly charged ion collision experiments is questionable.

From the various IEM calculations performed in this analysis, total cross sections in Kr collisions produced using a time-dependent target-response model [30] are most similar to those of H collisions. However, line-emission ratios from the no-response approximation are most consistent with the experimental ratios, while those produced using this target-response model are overall mixed. Previous analyses [25,26] that utilized the same response model also showed mixed agreements with the spectral counts. To move beyond this screening model but still work within the IEM, one may consider making use of the Krieger-Li-Iafrate approximation [46] in the OPM integral equation to obtain an accurate time-dependent exchange potential. A recent study of the He^+-He collision system showed the feasibility of such a calculation [47]. It would be worthwhile to explore the applicability of the Krieger-Li-Iafrate approximation in the context of collision-induced radiative emissions in future work.

ACKNOWLEDGMENTS

This work was funded by the Natural Sciences and Engineering Research Council of Canada (NSERC) under Grant No. RGPIN-2014-03611. High-performance computing resources for this work were provided by the Shared Hierarchical Academic Research Computing Network (SHARCNET). A.C.K.L. gratefully acknowledges the financial support from the Provost Dissertation Scholarship funded by York University (Canada).

[1] C. M. Lisse, K. Dennerl, J. Englhauser, M. Harden, F. E. Marshall, M. J. Mumma, R. Petre, J. P. Pye, M. J. Ricketts, J. Schmitt, J. Trumper, and R. G. West, Science **274**, 205 (1996).

[2] T. E. Cravens, Geophys. Res. Lett. **24**, 105 (1997).

[3] T. E. Cravens, Science **296**, 1042 (2002).

[4] D. Bodewits and R. Hoekstra, Phys. Rev. A **76**, 032703 (2007).

[5] R. K. Smith and N. S. Brickhouse, in *Advances in Atomic, Molecular, and Optical Physics*, edited by E. Arimondo, P. R. Berman, and C. C. Lin, Vol. 63, 1st ed. (Elsevier Academic Press, USA, 2014), p. 271.

[6] J. R. Machacek, D. P. Mahapatra, D. R. Schultz, Y. Ralchenko, A. Moradmand, M. O. A. El Ghazaly, and A. Chutjian, Astrophys. J. **809**, 75 (2015).

[7] P. Beiersdorfer, R. E. Olson, G. V. Brown, H. Chen, C. L. Harris, P. A. Neill, L. Schweikhard, S. B. Utter, and K. Widmann, Phys. Rev. Lett. **85**, 5090 (2000).
[8] J. B. Greenwood, I. D. Williams, S. J. Smith, and A. Chutjian, Phys. Rev. A **63**, 062707 (2001).
[9] R. Ali, P. A. Neill, P. Beiersdorfer, C. L. Harris, M. J. Raković, J. G. Wang, D. R. Schultz, and P. C. Stancil, Astrophys. J. **629**, L125 (2005).
[10] R. J. Mawhorter, A. Chutjian, T. E. Cravens, N. Djurić, S. Hossain, C. M. Lisse, J. A. MacAskill, S. J. Smith, J. Simcic, and I. D. Williams, Phys. Rev. A **75**, 032704 (2007).
[11] R. Ali, P. A. Neill, P. Beiersdorfer, C. L. Harris, D. R. Schultz, and P. C. Stancil, Astrophys. J. **716**, L95 (2010).
[12] R. J. Mawhorter, J. B. Greenwood, A. Chutjian, T. Haley, C. D. Mitescu, and J. Simcic, Phys. Rev. A **84**, 052714 (2011).
[13] M. Trassinelli, C. Prigent, E. Lamour, F. Mezdari, J. Mérot, R. Reuschl, J. Rozet, S. Steydli, and D. Vernhet, J. Phys. B **45**, 085202 (2012).
[14] X. Defay, K. Morgan, D. McCammon, D. Wulf, V. M. Andrianarijaona, M. Fogle, D. G. Seely, I. N. Draganić, and C. C. Havener, Phys. Rev. A **88**, 052702 (2013).
[15] M. Fogle, D. Wulf, K. Morgan, D. McCammon, D. G. Seely, I. N. Draganić, and C. C. Havener, Phys. Rev. A **89**, 042705 (2014).
[16] R. Ali, P. Beiersdorfer, C. L. Harris, and P. A. Neill, Phys. Rev. A **93**, 012711 (2016).
[17] V. Andrianarijaona, D. Wulf, D. McCammon, D. Seely, and C. Havener, Nucl. Instrum. Methods Phys. Res. Sect. B **350**, 122 (2015).
[18] D. G. Seely, V. M. Andrianarijaona, D. Wulf, K. Morgan, D. McCammon, M. Fogle, P. C. Stancil, R. T. Zhang, and C. C. Havener, Phys. Rev. A **95**, 052704 (2017).
[19] W. Fritsch and C. D. Lin, Phys. Rev. A **29**, 3039 (1984).
[20] R. Janev, R. Phaneuf, H. Tawara, and T. Shirai, At. Data Nucl. Data Tables **55**, 201 (1993).
[21] H. Ryufuku, K. Sasaki, and T. Watanabe, Phys. Rev. A **21**, 745 (1980).
[22] A. Leung, Ph.D. thesis, York University, 2018.
[23] M. Zapukhlyak, T. Kirchner, H. J. Lüdde, S. Knoop, R. Morgenstern, and R. Hoekstra, J. Phys. B **38**, 2353 (2005).
[24] A. Salehzadeh and T. Kirchner, J. Phys. B **46**, 025201 (2013).
[25] A. C. K. Leung and T. Kirchner, Phys. Rev. A **92**, 032712 (2015).
[26] A. C. K. Leung and T. Kirchner, Phys. Rev. A **93**, 052710 (2016).
[27] A. C. K. Leung and T. Kirchner, Phys. Rev. A **95**, 042703 (2017).
[28] J. D. Talman and W. F. Shadwick, Phys. Rev. A **14**, 36 (1976).
[29] K. Aashamar, T. M. Luke, and J. D. Talman, Atomic Data and Nuclear Data Tables **22**, 443 (1978).
[30] T. Kirchner, M. Horbatsch, H. J. Lüdde, and R. M. Dreizler, Phys. Rev. A **62**, 042704 (2000).
[31] T. Kirchner, M. Horbatsch, and H. J. Lüdde, Phys. Rev. A **64**, 012711 (2001).
[32] T. Kirchner, M. Horbatsch, and H. J. Lüdde, Phys. Rev. A **66**, 052719 (2002).
[33] O. J. Kroneisen, H. J. Lüdde, T. Kirchner, and R. M. Dreizler, J. Phys. A **32**, 2141 (1999).
[34] M. Horbatsch, Phys. Lett. A **187**, 185 (1994).
[35] T. Kirchner, H. J. Lüdde, M. Horbatsch, and R. M. Dreizler, Phys. Rev. A **61**, 052710 (2000).
[36] S. Martin, J. Bernard, L. Chen, A. Denis, and J. Désesquelles, Phys. Rev. Lett. **77**, 4306 (1996).
[37] L. J. Curtis, Am. J. Phys. **36**, 1123 (1968).
[38] S. M. Younger and W. L. Wiese, Phys. Rev. A **17**, 1944 (1978).
[39] S. Fritzsche, Comput. Phys. Commun. **183**, 1525 (2012).
[40] R. Janev, R. Phaneuf, and H. Hunter, At. Data Nucl. Data Tables **40**, 249 (1988).
[41] R. K. Janev and H. Winter, Phys. Rep. **117**, 265 (1985).
[42] L. Chen, J. Bernard, S. Martin, A. Denis, and J. Désesquelles, Phys. Rev. A **54**, 3049 (1996).
[43] T.-G. Lee, M. Hesse, A.-T. Le, and C. D. Lin, Phys. Rev. A **70**, 012702 (2004).
[44] S. Martin, J. Bernard, A. Denis, J. Désesquelles, L. Chen, and Y. Ouerdane, Phys. Rev. A **50**, 2322 (1994).
[45] E. Edgu-Fry, A. Wech, J. Stuhlman, T. G. Lee, C. D. Lin, and C. L. Cocke, Phys. Rev. A **69**, 052714 (2004).
[46] J. B. Krieger, Y. Li, and G. J. Iafrate, Phys. Rev. A **45**, 101 (1992).
[47] M. Baxter, T. Kirchner, and E. Engel, Phys. Rev. A **96**, 032708 (2017).